Fatigue experimental characterisation of brazed joints in aluminium microchannel heat exchangers

Federico Milan
Polytechnic Department of Engineering and Architecture, University of Udine, Via delle Scienze 206, Udine, 33100, Italy
milan.federico@spes.uniud.it, http://orcid.org/0009-0004-5684-7988

Sandro Ortolano, Gian Luca Gori
ThermoKey S.p.A., Via dell'Industria 1, Rivignano Teor, 33061, Italy
s.ortolano@thermokey.com, g.gori@thermokey.com

Denis Benasciutti, Enrico Salvati
Polytechnic Department of Engineering and Architecture, University of Udine, Via delle Scienze 206, Udine, 33100, Italy
denis.benasciutti@uniud.it, https://orcid.org/0000-0001-5999-5629
enrico.salvati@uniud.it, https://orcid.org/0000-0002-2883-0538

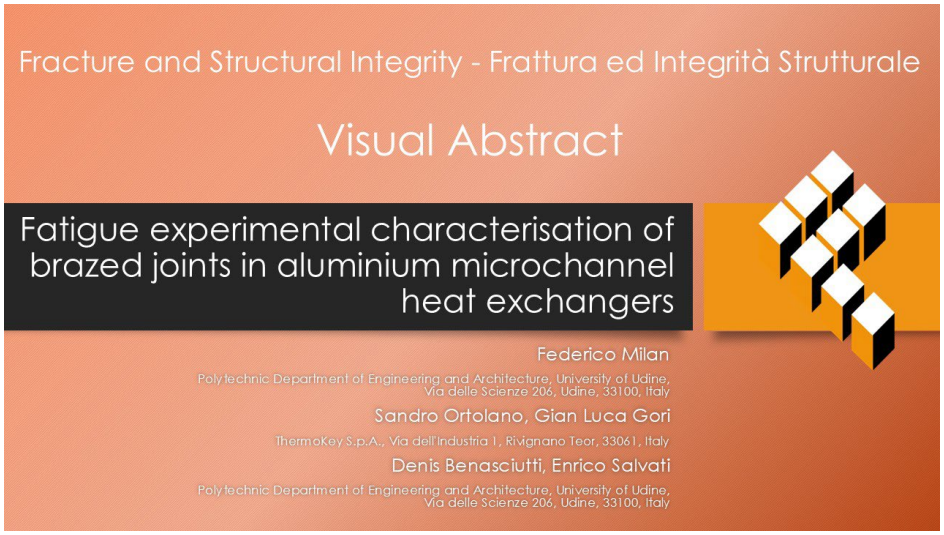

Citation: Milan, F., Ortolano, S., Gori, G. L., Benasciutti, D., Salvati, E., Fatigue experimental characterisation of brazed joints in aluminium microchannel heat exchangers, Fracture and Structural Integrity, 75 (2026) 167-178.

Received: 17.09.2025
Accepted: 17.10.2025
Published: 24.10.2025
Issue: 01.2026

KEYWORDS. Brazed joint, Microchannel heat exchanger, Fatigue, Aluminium alloy.

INTRODUCTION

Aluminium alloys play a central role in modern engineering applications due to their low density, good thermal conductivity, satisfactory mechanical performance, and corrosion resistance. These attributes have led to their widespread adoption in sectors such as automotive, energy, aerospace, and electronics, where weight reduction and

efficiency are critical design drivers. Among the various joining methods available for aluminium alloys, brazing has emerged as a particularly suitable solution for assembling complex heat exchanger components. Since the mid-1990s, the trend in automotive heat exchanger production has shifted from mechanical assembly toward brazing of aluminium alloys [1–3]. This shift has been driven by cost efficiency, improved safety, and recyclability, along with the superior sealing and durability that brazing can offer. Initially led by the automotive sector, this transition later extended to heating, air conditioning and refrigeration systems, where similar requirements apply.

Brazing is an efficient and cost-effective joining process that creates a permanent metallic bond between components through the melting and capillary-driven infiltration of a filler alloy, whose liquidus temperature lies below that of the base material but above 450 °C, thereby distinguishing it from soldering [1,4,5]. Compared to welding, brazing offers the important advantages of enabling the joining of dissimilar materials, minimizing thermal distortion due to uniform heating, and providing adequate joint strength for service applications [1,4–7].

Controlled-atmosphere brazing, in particular, has become the standard process for aluminium heat exchanger production [3,8]. The method relies on the use of 4xxx-series aluminium alloys as filler metals, applied either as clad sheets or brazing pastes, which melt and wet the base alloys during heating [1,9,10]. However, the process also presents significant challenges. The stable and refractory aluminium oxide film naturally present on aluminium surfaces must be disrupted to enable wetting by the molten filler. This is typically achieved through the use of fluxes, such as potassium fluoroaluminates, which dissolve the oxide layer and prevent its reformation during brazing [1,11,12]. In addition, the process must be tightly controlled, as partial dissolution of the core material, changes in microstructure, and diffusion of alloying elements can occur in the brazing zone, directly influencing the performance of the final joint [2,3].

Although the brazing process and its microstructural effects have been extensively studied, far fewer investigations have addressed the mechanical performance of such joints under service-like loading conditions. Consequently, the structural integrity of brazed joints under cyclic loading remains a scarcely addressed scientific and engineering concern. The presence of the brazed joint introduces local stress concentrations and can weaken the surrounding material, promoting crack nucleation [1]. As a result, the transition zone between the base metal and the brazed fillet often becomes the preferential site for mechanical damage initiation. In this context, the development of reliable methods for evaluating the fatigue life of brazed components is essential. However, although many brazed structures are routinely subjected to fatigue loads in service, standardised approaches for assessing their fatigue performance are still lacking.

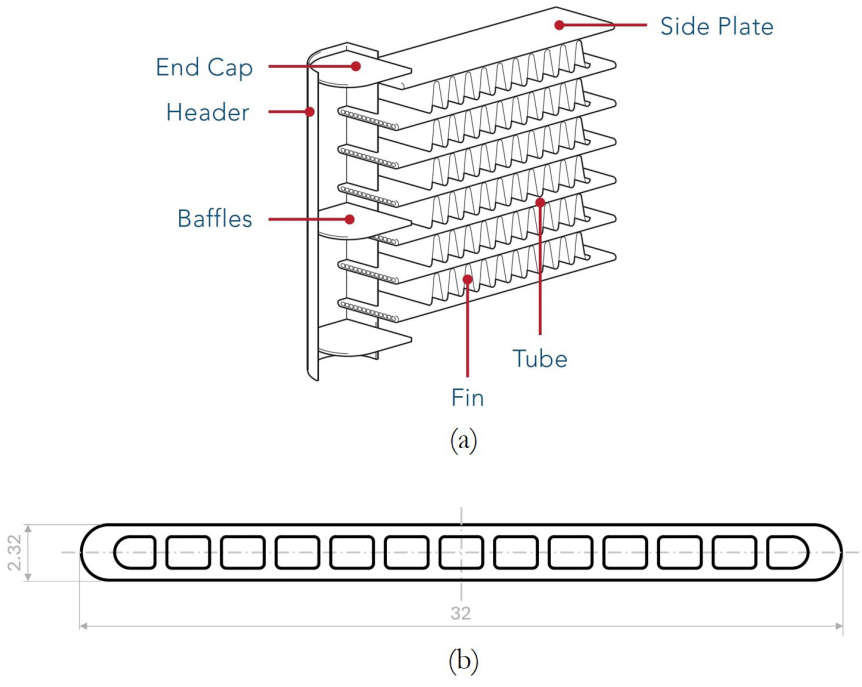

Figure 1: (a) Schematic representation of a typical microchannel heat exchanger, highlighting the main components. (b) Cross-sectional geometry of the multi-port tube investigated in this study (dimensions in millimetres).

This study presents an experimental investigation of the fatigue behaviour of brazed joints in microchannel heat exchanger (MCHE) components made of 3xxx-series aluminium alloys. A typical MCHE consists primarily of multi-port extruded

(MPE) tubes, folded headers, and louvered fins, which are joined together through a controlled-atmosphere brazing process. MPE tubes are flat aluminium profiles containing multiple parallel internal channels that enhance heat transfer by increasing the surface-to-volume ratio [13–15]. An example schematic of the MCHE configuration, based on a heat exchanger design by ThermoKey® and featuring a D-shaped header, is shown in Fig. 1a, together with the cross-sectional geometry of the multi-port tube investigated in this study (Fig. 1b). Only overall dimensions are shown to safeguard proprietary design information. These compact, high-efficiency heat exchangers are commonly used in refrigeration systems, where they are exposed to complex cyclic loading, primarily due to pressure fluctuations generated by compressors. Such loading conditions often involve stress cycles with varying amplitudes and mean stresses and can reach very high cycle counts over the operational life of the component. Therefore, ensuring the structural integrity of these joints under realistic service conditions is critical for safe and durable heat exchanger design.

To this end, the mechanical behaviour of both the base materials and the brazed joints was characterised through tensile testing and uniaxial fatigue testing, supported by Digital Image Correlation (DIC), Finite Element (FE) analysis, and Scanning Electron Microscopy (SEM) for post-mortem investigations.

MATERIALS AND METHODS

Materials

The specimens investigated in this study were extracted from aluminium MCHE components, specifically from headers and MPE tubes. The header and tube materials consisted of two different 3xxx-series aluminium alloys, both commonly used in heat exchanger applications due to their corrosion resistance and thermal conductivity [16–18]. The filler metal used for brazing was a 4xxx-series aluminium alloy, applied in brazing paste form to the joint area. Alloys of the 4xxx-series are commonly employed as brazing materials due to their low melting temperature and narrow melting range, which facilitate effective wetting and joint formation [1,10].

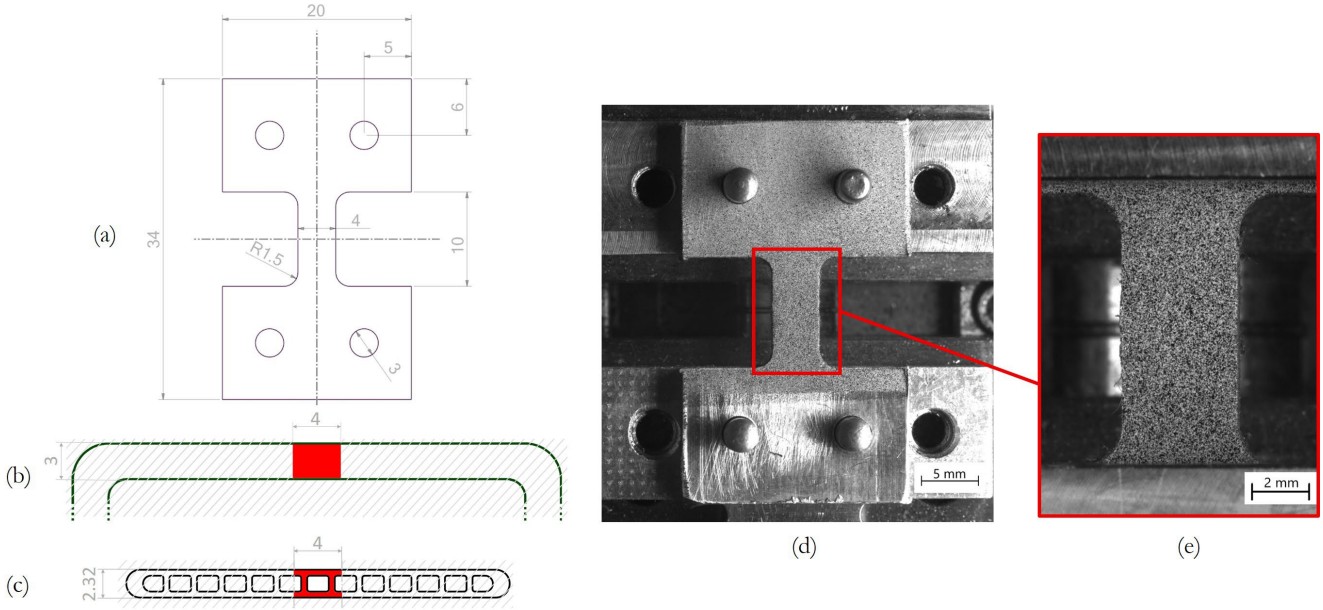

Figure 2: (a) Tensile specimen geometry (dimensions in millimetres). (b) Cross-sectional geometry of the gauge section of the specimen (highlighted in red) extracted from the header. (c) Cross-sectional geometry of the gauge section of the longitudinal specimen (highlighted in red) extracted from the MPE tube. (d) Tensile specimen positioned in the microtesting stage prior to loading. (e) Example of speckle pattern applied to the specimen surface for DIC analysis.

Tensile test on base materials

Tensile flat specimens were extracted from the header and tube.

Quasi-static tensile tests were performed using a Deben Microtest electromechanical testing system, consisting of a tensile stage and a corresponding control unit. The machine operates under displacement control, with a motor speed set to 0.2 mm/s. The tensile testing stage is equipped with a load cell with a capacity of 5 kN and a resolution of 0.1 mN.

The specimen geometry was designed based on the dimensional and load capacity constraints of the tensile stage (Fig. 2). Header specimens consisted of flat samples machined from the planar portion of the D-shaped header, with a nominal thickness of 3 mm, matching that of the original component (Fig. 2b). Tube specimens were extracted by machining the multi-port tube, and the resulting cross-sectional geometry of the gauge section is shown in Fig. 2c.
Surface preparation for DIC involved light polishing followed by the application of a thin white background layer, then overlaid with a fine black speckle pattern using an airbrush (Fig. 2e). Strain measurements were acquired using a custom 2D DIC setup consisting of a monochromatic camera with square pixels (5 MPixel resolution, 3.45 × 3.45 μm pixel size), a 50 mm fixed focal length lens, and an illumination system. The planar geometry of the specimens minimised out-of-plane displacements, allowing for reliable 2D strain field evaluation [19].
Two material conditions were considered for both the header and the tube:

- As-received (non-brazed) condition, representing the base materials without any thermal exposure.
- Heat-treated condition, in which specimens underwent the full brazing thermal cycle without the application of filler metal or actual joining.

This heat treatment was performed to evaluate the effect of the brazing cycle on the mechanical behaviour of the base materials. Both header and tube samples were subjected to the same furnace thermal cycle, which followed the industrial brazing procedure used for actual heat exchanger fabrication. The objective was to characterise any thermally induced degradation of the mechanical properties of the base material caused solely by thermal exposure, independently of the presence of the brazed joint. The heat treatment was carried out in a controlled-atmosphere brazing furnace, using a peak temperature of 595 °C and a holding time of approximately 4 minutes at peak, followed by controlled cooling. The complete temperature profile is illustrated in Fig. 3.

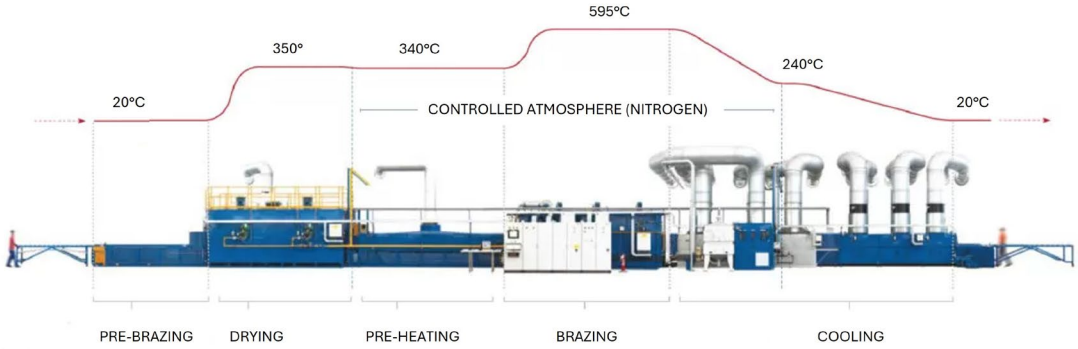

Figure 3: Schematic of the brazing thermal cycle.

The header and tube components were fabricated using two different forming processes: the headers were manufactured by lamination (rolling), while the tubes were produced by extrusion. To account for possible anisotropy in mechanical properties, specimens for tensile testing were extracted from two orientations relative to the processing direction (Fig. 4):

- Longitudinal: parallel to the lamination or extrusion direction.
- Transverse: perpendicular to the lamination or extrusion direction.

This allowed for a comparative assessment of how the forming process and anisotropic microstructure affect the strength of the materials, both in the as-received condition and after the thermal cycle replicating the brazing process.
A total of three tensile specimens were tested for each material condition and orientation. Mechanical properties—such as ultimate tensile strength (UTS), yield strength, and elongation at break—were calculated as the mean value of the three replicated measurements.
To obtain a representative stress-strain curve, the same DIC strain grid was defined for each specimen configuration. Each individual curve was first truncated at the point of maximum stress to exclude post-necking behaviour. The truncated curves were then interpolated onto the common strain grid, and the mean curve was computed by averaging the interpolated stress values at each strain point.

Fatigue specimen design

To accurately assess the fatigue behaviour of the brazed joints resembling realistic operating conditions, an experimental uniaxial fatigue characterisation was carried out by a precise design of tested samples. To ensure these fatigue samples could reproduce the actual cyclic stress state in the joint region, it was first necessary to characterise the mechanical cyclic stress

state of the real component under service-like loading. To effectively serve this purpose, a bespoke experimental investigation was pursued, followed by a corresponding FE numerical analysis that exploits local strain assessment of the experiments for its validation. The validated FE model was then used to attain a more comprehensive evaluation of the strain and stress field in the regions of interest and therefore to assess whether a uniaxial fatigue test characterisation can be representative of the actual cyclic stress state experienced by the heat exchanger when in service.
The physical prototype of a simplified microchannel heat exchanger was fabricated and instrumented with strain gauges (Fig. 5). The simplified geometry included headers with a standard cross-section but reduced length, and two multi-port tubes positioned at the header ends. The prototype was subjected to internal pressure representative of operating conditions, and the strain-gauge measurements recorded the local strain in the proximity of the most critical region, i.e. brazed region close to the lateral end of the MPE tube.

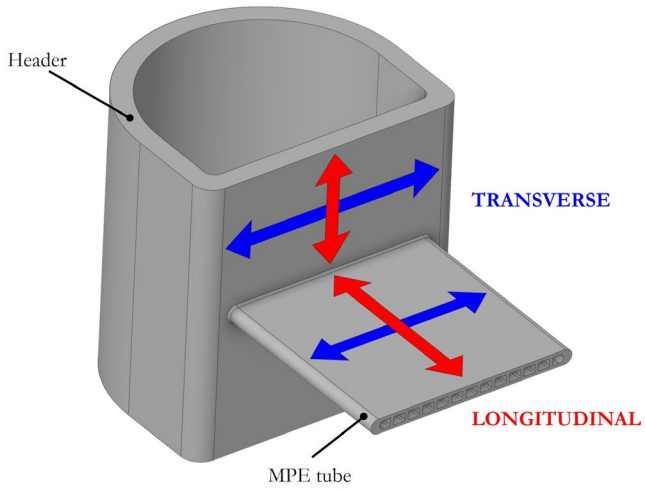

Figure 4: Schematic of a microchannel heat exchanger section showing the header and MPE tube components, with the longitudinal and transverse orientations relative to the forming directions indicated.

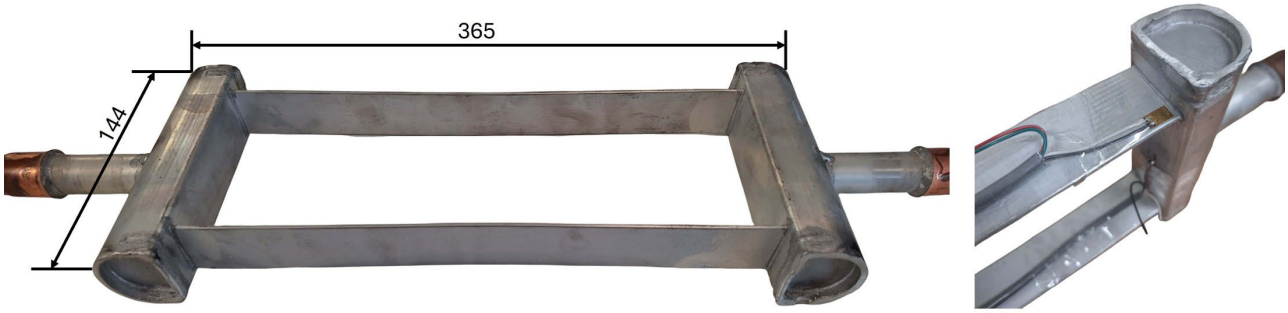

Figure 5: (a) Prototype of the microchannel heat exchanger with simplified geometry (dimensions in millimetres). (b) Prototype instrumented with strain gauges for FE model validation.

Secondly, a linear-elastic FE analysis of a simplified microchannel heat exchanger geometry was implemented and solved. The FE model was built to replicate the geometry of the simplified MCHE prototype. The FE mesh primarily consisted of second-order tetrahedral elements. However, to improve accuracy near the outer surface of the tube, three structured layers of second-order hexahedral elements were implemented in that region. Additionally, due to the complex geometry of the tube, a limited number of wedge and pyramid elements were introduced to ensure mesh continuity. The minimum element edge length in the joint region was approximately 0.05 mm, providing sufficient resolution of local stress gradients, while coarser elements (up to 0.7 mm) were employed in less critical areas to reduce the computational effort.
By exploiting geometric and mechanical symmetries, only one-eighth of the assembly was modelled (Fig. 6).

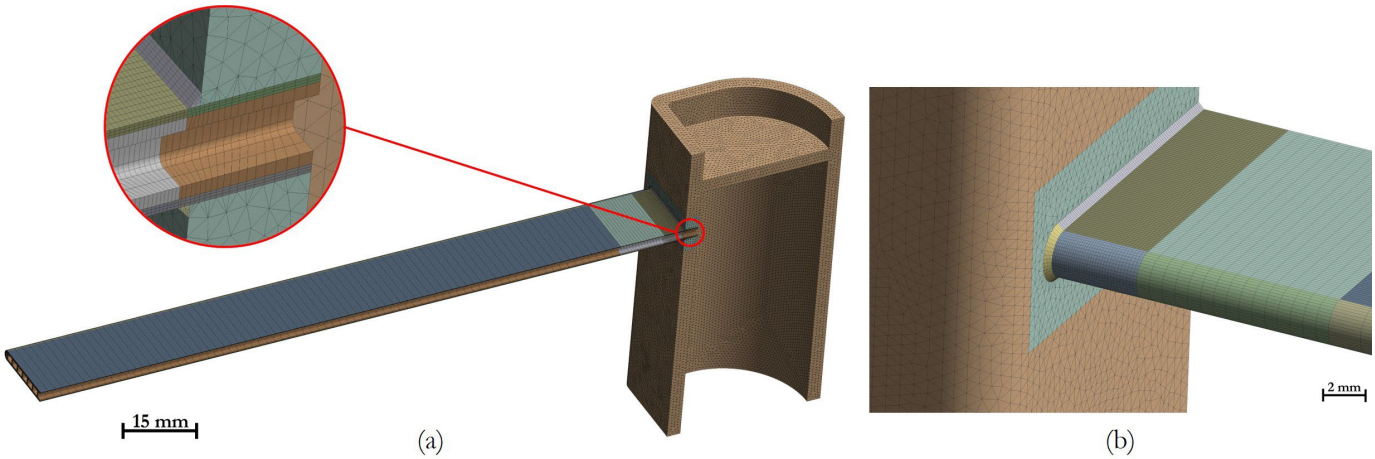

Figure 6: (a) Finite element mesh of the simplified heat exchanger assembly. (b) Detail of the joint region in the finite element mesh.

The assembly was subjected to internal pressure mimicking in-service loading conditions. The brazing fillet was modelled with a sharp edge, both to simplify the geometry and due to the lack of detailed information about the actual fillet profile. In practice, the joint geometry is not perfectly homogeneous, and its precise shape can vary due to local variations in filler metal distribution. Moreover, modelling a sharp edge represents a conservative assumption, as it accounts for the worst-case scenario in terms of stress concentration. The authors acknowledge that this idealised representation introduces a stress singularity at the toe of the fillet, making the absolute stress values at the notch tip not physically representative. Nevertheless, the simulation results are still valuable, as they clearly highlight the region of highest stress concentration near the joint, which is critical for identifying potential crack initiation sites. The numerical results revealed a clear concentration of tensile stress at the toe of the brazed fillet, particularly at the lateral edge of the tube (see Fig. 7). It should be emphasised, however, that due to the geometric idealisation adopted, the absolute von Mises stress values predicted near the sharp edge of the brazed fillet are not physically meaningful and should only be interpreted as indicative of the location of the stress concentration.

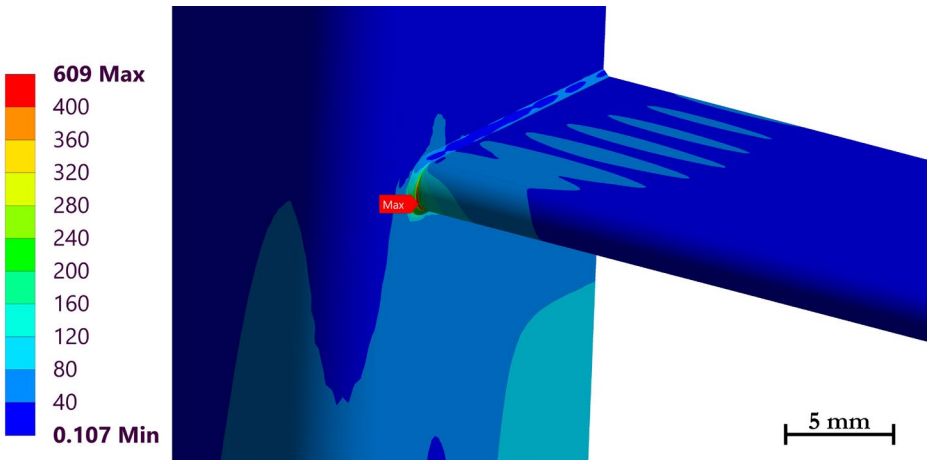

Figure 7: Detail of the FE model of the simplified microchannel heat exchanger section, showing the von Mises stress distribution (MPa).

The observation obtained through the calibrated FE model guided the design of a fatigue specimen that could replicate the local joint geometry and critical stress field under uniaxial cyclic loading. A brazed structural detail for fatigue testing was designed based on an FE analysis, incorporating a brazed joint between the tube and header materials. To ensure meaningful testing, the specimen geometry was designed to replicate the actual joint configuration as closely as possible, retaining the essential geometric features of the multi-port tube and the header (Fig. 8). The specimens were brazed using the same controlled-atmosphere furnace cycle described in the previous section. Brazing paste was applied in the joint area to ensure proper metallurgical bonding.

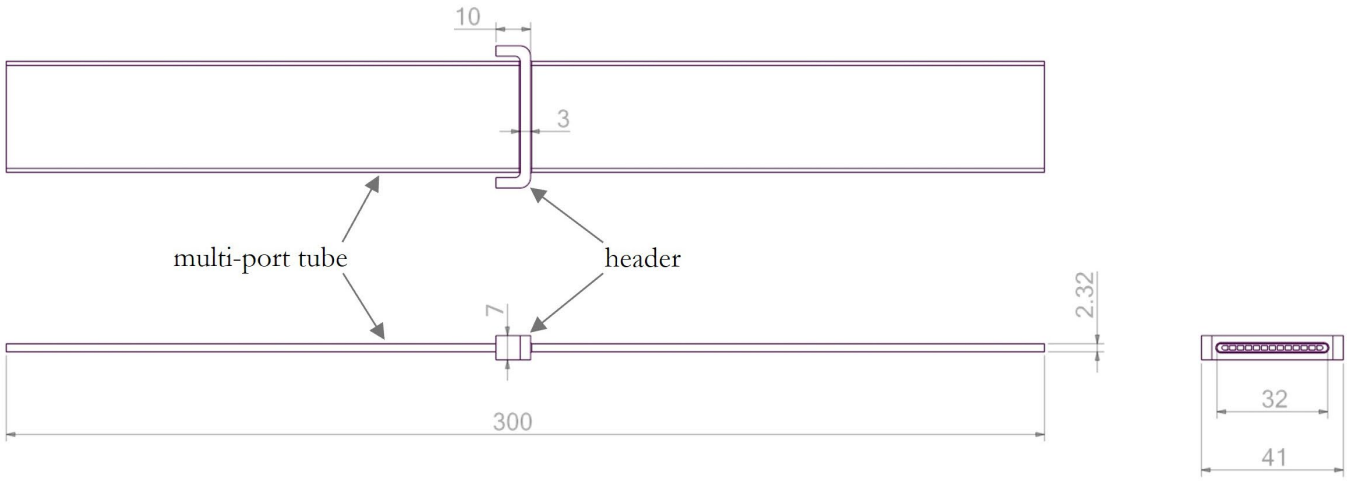

Figure 8: Fatigue specimen geometry (dimensions in millimetres).

Fatigue testing

After fabrication, the specimens were tested under sinusoidal axial loading at constant stress amplitude using a STEP Lab EA050 electromechanical fatigue testing machine. All tests were performed at a stress ratio R=0.1 and a frequency of 20 Hz.

Fatigue test data were used to determine both the nominal stress range threshold corresponding to the endurance limit and the fatigue behaviour in the finite life region of high-cycle fatigue, allowing estimation of the mean S–N curve and its scatter band.

The fatigue endurance of the brazed joint specimens was estimated by the staircase (up-and-down) method, targeting a run-out threshold of 10^7 cycles as the criterion for the material endurance limit [20]. The initial load level was chosen based on preliminary tests and decreased or increased by a fixed increment of 100 N of the maximum applied load depending on whether the previous sample failed or survived. A total of 12 specimens were tested following this protocol. The resulting binary sequence of failures and non-failures was analysed using the Dixon-Mood statistical method to estimate the mean endurance limit and associated standard deviation. This method assumes a log-normal distribution of fatigue life and is suitable for small sample sizes and stepwise loading procedures [20,21].

In addition to the estimated mean endurance limit, lower-bound values associated with specific reliability and confidence levels were also determined. These were calculated using the one-sided lower-bound tolerance limit approach.

Fractographic analysis using SEM was performed on selected specimens that failed before reaching the run-out threshold to observe the crack initiation behaviour and characterise the crack path through the joint.

RESULTS AND DISCUSSION

Tensile behaviour of base materials

Representative engineering stress-strain curves for each material and condition are shown in Fig. 9. Both the tube and header materials exhibited a modest difference between the longitudinal and transverse directions, with the longitudinal specimens generally displaying higher strength compared to their transverse counterparts, under the same heat treatment conditions.

The heat treatment simulating the brazing cycle had opposite effects on the two materials:

- For the header material, heat treatment led to a significant reduction in both yield strength and ultimate tensile strength.
- In contrast, the tube material showed a modest increase in strength after the thermal cycle.

This opposite trend can be rationalised by considering the different initial processing routes and microstructural conditions of the two alloys. Although both belong to the 3xxx-series, the extruded tube material retains a fibrous, strain-hardened microstructure with a higher degree of solid-solution strengthening, which can be partially stabilised or even slightly hardened by diffusion and precipitation phenomena during the brazing thermal cycle. Conversely, the rolled header alloy, initially in a cold-worked state, is more prone to recovery and recrystallisation under the same thermal exposure, leading to

softening and reduced tensile strength. These microstructural mechanisms are consistent with the observed opposite effects of the brazing heat treatment on the mechanical properties of the two components.
A summary of key mechanical properties extracted from the tests is provided in Tab. 1.

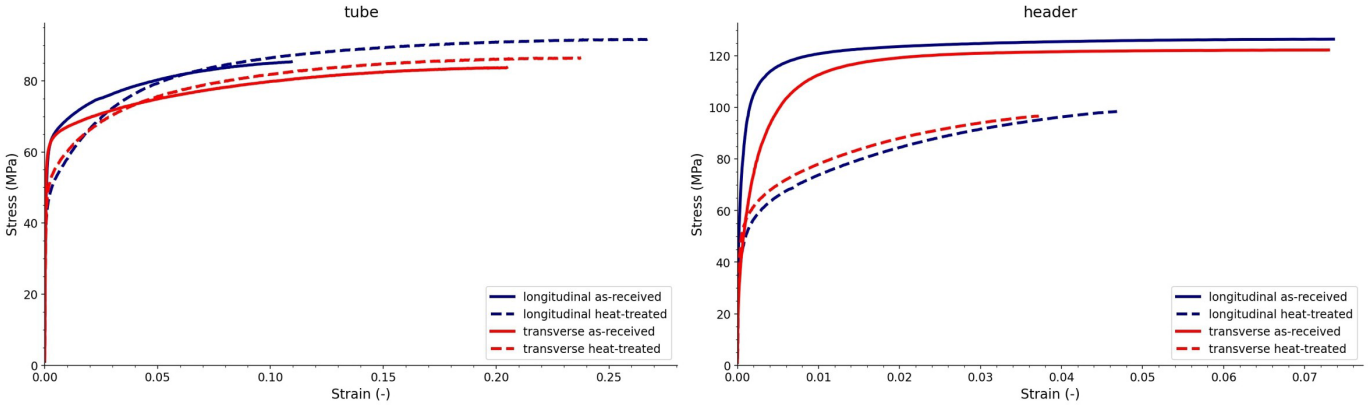

Figure 9: Representative engineering stress-strain curves of (a) MPE tube and (b) header materials in as-received and heat-treated conditions, for both longitudinal and transverse orientations.

Material	Orientation	Condition	σ_{UTS} (MPa)	$R_{p0.2\%}$ (MPa)	ε_b (%)
MPE Tube	Longitudinal	As-received	86.1	63.7	15.1
	Longitudinal	Heat-treated	90.4	48.8	27.8
	Transverse	As-received	81.6	57.9	22.2
	Transverse	Heat-treated	85.0	57.7	20.8
Header	Longitudinal	As-received	128.0	110.9	8.0
	Longitudinal	Heat-treated	105.9	63.9	14.1
	Transverse	As-received	121.1	93.5	9.0
	Transverse	Heat-treated	100.2	66.2	4.4

Table 1: Summary of tensile properties for MPE tube and header materials in different conditions and orientations.

Fatigue behaviour of brazed joints

Due to the complex geometry near the joint, including geometric irregularities and potential stress singularities, the local stress state could not be accurately defined. For this reason, fatigue results are reported in terms of nominal stress, calculated by dividing the applied force by the minimum cross-sectional area of the specimen, without accounting for the presence of the brazed joint or local geometric effects. This approach allows for consistent comparison between specimens while acknowledging that local stress values in the joint cannot be reliably determined.
The fatigue test results of the brazed joint specimens, including the finite life region and the run-out tests, are summarised as a $\Delta\sigma_{nom}$–Life diagram in Fig. 10.
The outcome of each test (failure or run-out) included in the staircase procedure is summarised in Fig. 11, along with the corresponding nominal stress ranges.
Based on the observed failure sequence and the load increments used during the testing, the estimated endurance limit, calculated using the Dixon-Mood statistical method, was found to be $\Delta\sigma_{e,nom}$=60.0 MPa, with an associated standard deviation of 2.0 MPa. $\Delta\sigma_{e,nom}$ represents the nominal stress range that the joint can withstand for 10^7 cycles under the given loading conditions (R=0.1) with a 50% survival probability. The lower-bound endurance limits corresponding to a 90% confidence level and 10% and 90% reliability were found to be $\Delta\sigma_{e,nom,90,10}$=64.9 MPa and $\Delta\sigma_{e,nom,90,90}$=55.1 MPa, respectively. The lower-bound endurance limit $\Delta\sigma_{e,C,R}$ is defined as the stress range level that, with a confidence level of C%, is expected to be exceeded by R% of the population [20].

The relatively low fatigue endurance limit, compared to the monotonic tensile strength of the base material of the tube, reflects the detrimental effect of stress intensification and metallurgical heterogeneity at the brazed joint, confirming its role as the dominant fatigue-critical region.

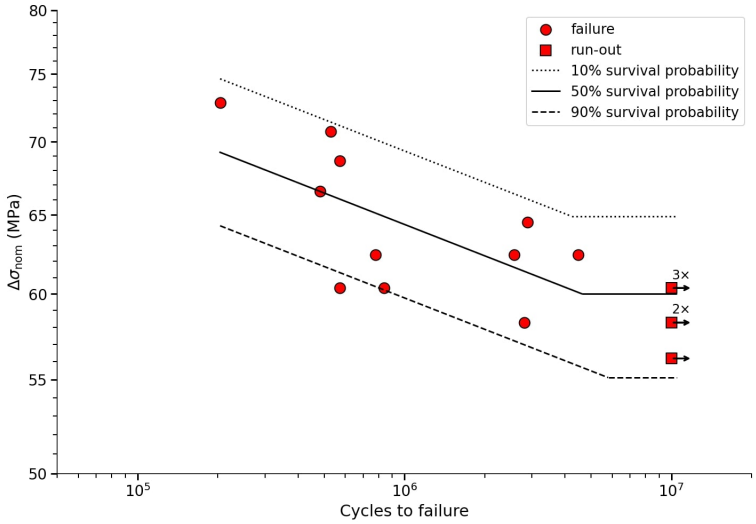

Figure 10: $\Delta\sigma_{nom}$–Life plot for brazed joint fatigue specimens.

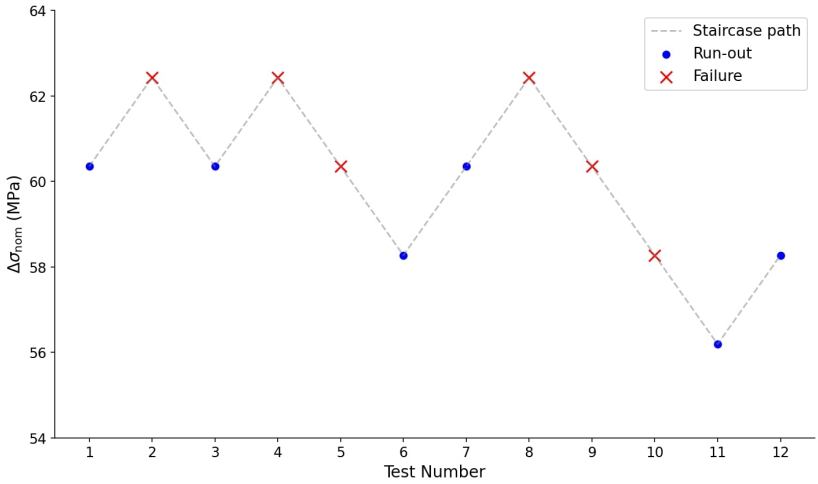

Figure 11: Schematic staircase fatigue test results performed on specimens with brazed joint (run-out threshold: 10^7 cycles).

Fractographic analysis of failed specimens (Fig. 12) revealed that crack initiation consistently occurred at the brazed joint toe, specifically at the lateral edge of the tube. This location corresponds to a high-stress region identified in the FE simulations of the simplified heat exchanger geometry. Moreover, this crack initiation site closely matches the area where in-service failures have been observed in actual heat exchanger components, reinforcing the relevance of the chosen specimen geometry and loading mode.

SEM analysis revealed the following typical high-cycle fatigue features:

- Crack initiation occurred at the surface, along the lateral edge of the tube, near the brazed fillet toe.
- Ratchet marks were observed in the crack propagation zone.
- Final failure regions exhibited characteristics of ductile failure.

Additional SEM observations revealed the presence of small particles near the surface, particularly in the vicinity of the crack initiation zone (Fig. 12a and Fig. 12c). The chemical composition of these features was characterised via Energy-Dispersive X-ray Spectroscopy (EDS), performed during SEM analysis. These particles were found to contain mainly fluorine (F), potassium (K), aluminium (Al), and caesium (Cs), elements that match the composition of the brazing paste used in the joining process. This suggests that the particles are likely inclusions originating from the brazing material.

As only a limited number of fracture surfaces were analysed, a comprehensive statistical assessment of the inclusion size and distribution was not possible. However, quantitative estimates of the inclusion size were obtained for several observed defects using Murakami's $\sqrt{area}$ parameter (i.e., the square root of the projected inclusion area [22]), yielding $\sqrt{area}$ values in the range of approximately 75–80 μm. These estimates provide an indicative measure of the defect scale at crack initiation sites and highlight their potential role in promoting local stress concentration. Although their exact role remains to be fully quantified, the observation of such inclusions near the joint surface suggests that they may act as preferential fatigue crack initiation sites, underlining the importance of strict control of the brazing process in fatigue-critical applications.

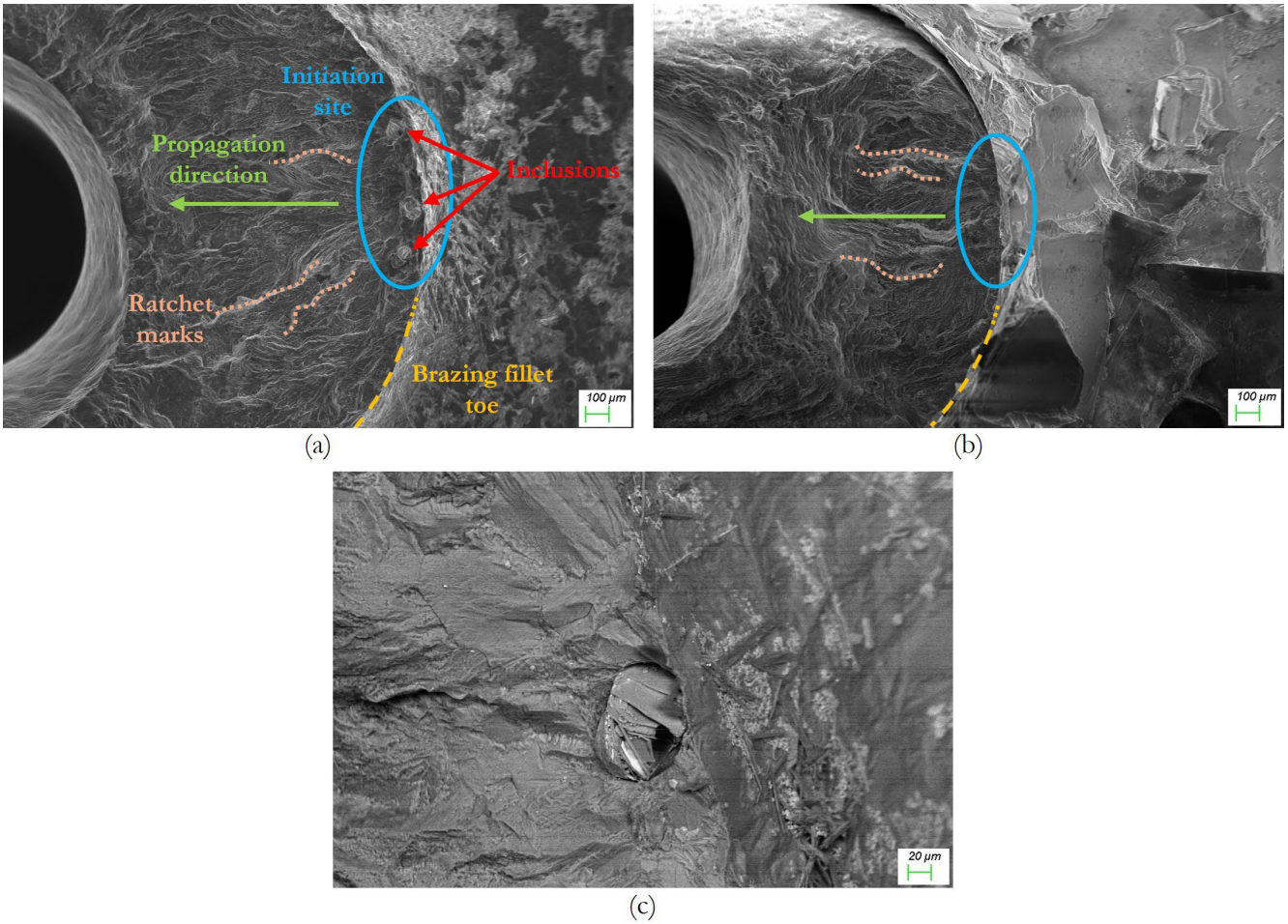

Figure 12: (a), (b) SEM images of fracture surfaces from fatigue-tested brazed joint specimens (secondary electron mode). (c) SEM image showing a sub-surface particle located in the crack initiation area at the lateral edge of the brazed joint. (backscattered electron mode)

Conclusions

This study investigated the tensile and fatigue behaviour of aluminium brazed joints in components representative of microchannel heat exchangers, specifically involving headers and multi-port tubes. Tensile tests, supported by DIC, highlighted the effect of the thermal cycle of the brazing process, which significantly reduces the strength of the header material while slightly increases that of the tube material. Representative uniaxial fatigue tests on specimens containing a representative brazed joint, designed on a bespoke FE stress analysis, revealed that fatigue failure consistently initiated at the brazed fillet toe, near the lateral edge of the multi-port tube. This location corresponds to the highest local stress concentration region predicted by simulation and aligns with observed failure sites in real components. Due to geometric singularities at the brazed region, fatigue performance was evaluated in terms of applied force rather than local stress. SEM observations of specimen fractured surfaces confirmed typical high-cycle fatigue features—including surface

crack initiation, ratchet marks, and final ductile failure—along with the presence of secondary particles enriched in F, K, Al, and Cs, consistent with inclusions introduced during the brazing process. Overall, the findings emphasise the critical influence of joint geometry, local microstructure, and manufacturing conditions on fatigue performance, underlining the need for tailored design and quality control strategies in brazed aluminium structures.

ACKNOWLEDGEMENTS

The authors acknowledge that this research was funded by the European Union - Next Generation EU PNRR, Mission 4, Component 2, Investment 3.3, CUP G23C23001170005.
The authors also gratefully acknowledge Mr. Francesco Sordetti and Prof. Alex Lanzutti for their assistance with the SEM analyses and Ms. Odeta Shyti for valuable experimental support during her internship at ThermoKey.

REFERENCES

[1] American Welding Society (2007). Brazing Handbook, 5th ed., Miami, American Welding Society.
[2] Lacaze, J., Tierce, S., Lafont, M.C., Thebault, Y., Pebere, N., Mankowski, G., Blanc, C., Robidou, H., Vaumousse, D. and Daloz, D. (2005). Study of the microstructure resulting from brazed aluminium materials used in heat exchangers, Mater. Sci. Eng.: A, 413-414, pp. 317–321. DOI: https://doi.org/10.1016/j.msea.2005.08.187
[3] Norouzi Afshar, F., de Wit, J.H.W., Terryn, H. and Mol, J.M.C. (2012). The effect of brazing process on microstructure evolution and corrosion performance of a modified AA4XXX/AA3XXX brazing sheet, Corrosion Science, 58, pp. 242-250. DOI: https://doi.org/10.1016/j.corsci.2012.01.030
[4] Jacobson, D.M. and Humpston, G. (2005) Principles of brazing, ASM International. DOI: https://doi.org/10.31399/asm.tb.pb.9781627083515
[5] Way, M., Willingham, J., Goodall, R. (2020). Brazing filler metals, International Materials Reviews, 65(5), pp. 257-285. DOI: https://doi.org/10.1080/09506608.2019.1613311
[6] Filliard, G., El Mansori, M., Tirado, L., Mezghani, S., Bremont, C. and De Metz-Noblat, M. (2017). Industrial fluxless laser weld-brazing process of steel to aluminium at high brazing speed. Journal of Manufacturing Processes, 25, pp. 104–115. DOI: https://doi.org/10.1016/j.jmapro.2016.12.002
[7] Suganuma, K. and Kawakami, N. (1993). Novel processing of brazing aluminium to aluminium and to austenitic stainless steel, Materials Science and Technology, 9(4), pp. 349-358. DOI: https://doi.org/10.1179/mst.1993.9.4.349
[8] Sugiyama, Y. (1989). Brazing of aluminium alloys, Welding International, 3(8), pp. 700–710. DOI: https://doi.org/10.1080/09507118909446642
[9] Bai, X., Zhao, F., Huang, W., Du, X., Liu, Y. and Zhu, D. (2025). Interfacial microstructure evolution and fracture mechanism of 6063 aluminum alloy joints vacuum brazed with Al-Si-Mg filler metal. Engineering Failure Analysis, 180, 109879. DOI: https://doi.org/10.1016/j.engfailanal.2025.109879
[10] Nayeb-Hashemi, H. and Lockwood, M. (2002). The effect of processing variables on the microstructures and properties of aluminum brazed joints, Journal of Materials Science, 37, pp. 3705-3713. DOI: https://doi.org/10.1023/A:1016517510260
[11] Markovits, T., Takács, J., Lovas, A. and Belt, J. (2003). Laser brazing of aluminium, Journal of Materials Processing Technology, 143–144, pp. 651–655. DOI: https://doi.org/10.1016/S0924-0136(03)00310-8
[12] Mirski, Z., Pabian, J., Wojdat, T. and Hejna, J. (2020). Significance of the brazing gap in the brazing of aluminium heat exchangers for automotive industry, Weld. Tech. Rev., 92, pp. 7–14. DOI: https://doi.org/10.26628/wtr.v92i4.1114
[13] Khan, M.G. and Fartaj, A. (2011). A review on microchannel heat exchangers and potential applications, Int. J. Energy Res., 35, pp 553-582. DOI: https://doi.org/10.1002/er.1720
[14] Hayase, G. (2016). Development Of Micro Channel Heat Exchanger For Residential Air-Conditioners, International Refrigeration and Air Conditioning Conference, 1566.
[15] Bhosale, S.S. and Acharya, A.R. (2020). Review On Applications of Micro Channel Heat Exchanger, Int. Res. J. Eng. Technol., 07(04), pp. 5326–5329. DOI: https://doi.org/10.13140/RG.2.2.31044.65922
[16] Cao, Q., Zhao, N., Xia, C., Zhang, Z., Cheng, L. and Zhou, D. (2025). Effect of brazing and artificial aging on the microstructure and mechanical properties of a high-strength four-layer laminar aluminum alloy, Vacuum, 239, 114388. DOI: https://doi.org/10.1016/j.vacuum.2025.114388

[17] Xia, C., Deng, S., Ni, C., Ji, Y., Zheng, W., Luo, J., Xu, W., Li, W. and Pang, Y. (2023). Study on laminar structure and process on high strength brazed aluminum alloy for heat exchangers, Vacuum, 215, 112303. DOI: https://doi.org/10.1016/j.vacuum.2023.112303

[18] Yuan, Z., Lu, Y., Tu, Y., Wang, X., Ni, Z., Peng, J., Chen, X., Yu, H., Raza, S.R.A. and Yin, S. (2025). Mechanism of liquid film migration and interface reaction in multi-layer aluminum sheets during brazing based on the homogenization annealing, Journal of Materials Research and Technology, 38, pp. 5166–5179. DOI: https://doi.org/10.1016/j.jmrt.2025.08.264

[19] International Digital Image Correlation Society, Jones, E.M.C. and Iadicola, M.A. (Eds.) (2018). A Good Practices Guide for Digital Image Correlation. DOI: https://doi.org/10.32720/idics/gpg.ed1

[20] Lee, Y.L., Pan, J., Hathaway, R.B., Barkey, M.E. (2005). Fatigue testing and analysis: theory and practice, Elsevier Butterworth-Heinemann. DOI: https://doi.org/10.1016/B978-0-7506-7719-6.X5000-3

[21] Dixon, W.J. and Mood, A.M. (1948). A Method for Obtaining and Analyzing Sensitivity Data, Journal of the American Statistical Association, 43(241), pp. 109–126. DOI: https://doi.org/10.2307/2280071

[22] Murakami, Y. (2019). Metal fatigue: Effects of small defects and nonmetallic inclusions, 2nd ed., Academic Press. DOI: https://doi.org/10.1016/C2016-0-05272-5